Heliyon 8 (2022) e12175

Contents lists available at ScienceDirect

Heliyon

journal homepage: www.cell.com/heliyon

Research article

# Properties of flame-retardant leaf fiber cement-based composites at high temperatures

Demin Jiang [a,*], Haodong Xu [a], Shuchen Lv [a], Di Jiang [c], Suping Cui [b], Shiguo Sun [a], Xiaoruan Song [a], Shiqin He [a], Jingzong Zhang [a]

[a] College of Civil Engineering, North China University of Technology, Beijing 100144, PR China
[b] College of Materials Science & Engineering, Beijing University of Technology, Beijing 100124, PR China
[c] College of Architecture and Art, North China University of Technology, Beijing 100144, PR China

ARTICLE INFO

*Keywords:*
Leaf fiber
Flame retardant modification
Cement-based composites
High temperatures
Properties

ABSTRACT

Flame retardant modification of leaf fibers was carried out to solve the technical problem of poor fire resistance of plant fibers and improve the utilization rate of urban fallen leaves in building materials. The modification scheme adopts three flame retardants, i.e., ammonium polyphosphate (APP), magnesium hydroxide (MH), and aluminum hydroxide (ATH), and two covering layers, i.e., pure acrylic polymer lotion and water glass ($Na_2O \cdot nSiO_2$) solution. The modified leaf fiber's combustion behavior and pyrolysis properties were tested and analyzed. The physical and mechanical characteristics, as well as the thermal insulation qualities, of leaf fiber cement-based composites (LFCC) were studied at high temperatures. The findings revealed that the three flame retardants had an effect on the chemical structure of leaf fibers. In comparison to leaf fibers without flame-retardant modification, flame-retardant-modified leaf fibers have a much greater thermal stability. and its LOI is greater than 27.0%, which is a fire-retardant material. Except for the sample with water glass as the modified cover layer, at high temperatures, the composite flame-retardant fiber LFCC's mass-loss rate is lower compared with fibers without flame-retardant modification or fibers modified with only one kind of flame-retardant. In the composite flame-retardant modified fiber LFCC, the samples with better strength at high temperature are those with ATH replacing 30% and 50% MH. The thermal conductivity of LFCC is negatively correlated with the range of temperature change.

## 1. Introduction

Currently, the research on improving the flame retardancy of fiber composites through the modification of plant fibers worldwide mainly focuses on papermaking materials, fiber resin matrix composites, wood plastic composites, and so on. Faseha Shukor et al. [1] studied the effect of ammonium polyphosphate on flame retardancy, thermal stability, and mechanical properties in alkali-treated kenaf fiber/polylactic acid (PLA) biological composites. K. Ramanaiah et al. [2] studied the mechanical properties, thermophysical properties, and flammability of sargassum fiber/polyester composites. Nannan Li et al. [3] studied the flame retardant and reinforcement modification of ramie/polyethylene composites through surface treatment of ramie fabrics. However, in most literature, the flame-retardant modification of plant fibers is limited to wood flour fiber, flax fiber, sisal fiber, etc. No reports on the flame retardancy of leaf fiber cement-based composites.

According to statistics, the number of fallen leaves in the cities increases yearly in autumn. The weight of fallen leaves from Beijing and its surrounding areas alone is more than 100 tons per day. Such a spectacular scene lasts about a month, while the number of leaves falling at the peak is about 3,000 tons per day in downtown Beijing [4]. The primary research and applications of leaves have focused on producing fertilizer, feed, and medicine in China. However, few research and applications have used leaves as a building material. Most cities and regions do not have adequate conditions to turn leaves into fertilizers, so most fallen leaves are transported to garbage dumps to be burnt or buried. The burning debris will produce many floating dust and carcinogenic substances, such as tribenzopyrene and tetrabenzopyrene, increasing particulates in the air [5], and severe air pollution, severely impacting people's health. Nearly 30%–40% of the fallen leaves cannot be recycled, causing environmental pollution. Therefore, it is a new subject for scientific research workers to turn their attention to fallen leaves in the

* Corresponding author.
*E-mail address:* jdm2004@126.com (D. Jiang).

https://doi.org/10.1016/j.heliyon.2022.e12175
Received 4 January 2022; Received in revised form 7 May 2022; Accepted 29 November 2022

cities and find ways of turning them into treasures to reduce urban smog weather and beautify the urban environment.

Plant fiber cement-based composites are a kind of green environment-friendly building material made of cement as the cementation material and plant fibers as reinforcing material through a series of technological processes and cement hydration and hardening [6, 7].

If the fallen leaf fibers are applied to cement-based composite materials, and the composite materials are widely used in construction, it would be a powerful way to solve recycling fallen leaf fibers [8, 9]. In thermal insulation building materials, we can fully use the light, porous and thermal insulation characteristics of fallen leaf fibers to make thermal insulation materials alone or combined with other materials [10].

As a natural high molecular polymer, plant fibers will degrade thermally at a certain temperature. Thermal degradation first destroys fibers' structure and then affects the strength and other properties of the composite material. Additionally, plant fibers prone to igniting fiercely in flame because its combustible properties, creating a large amount of smoke and hazardous fumes [11] and cause inflicting injuries and financial damage. Plant fibers' poor fire resistance performance is one of the most significant shortcomings limiting their application in construction. To reduce the hazards and losses of fire and prevent catastrophic fires, countries worldwide are generally concerned about developing and producing flame retardants and flame-retardant plant fibers. Plant fiber composite wall materials' flame retardancy has attracted more attention [12]. In plant fiber cement-based composite materials, plant fibers are encased in cement substrate, this situation will adjourn or greatly reduces the fibers' flammability. There is still more research that needs to be done on the mechanical and physical properties of plant fiber cement-based composite materials at high temps.

To boost the usage rate of fiber plants in buildings, the technical issue of their low flame-proof performance must be addressed. Modifying fiber plants and treating flame retardants are critical to resolving this issue [13].

In this paper, the raw material was the fallen leaves in the cities with enormous output in China. The research object, fibers made from poplar leaves, and we modify the fibers using a variety of flame retardants. The combustion behavior and pyrolysis performance of leaf fiber and leaf fiber cement-based composites (LFCC) were tested and analyzed. It was investigated how modified leaf fiber affected the properties of LFCC at high temps. The changes to the modified leaf fiber's chemical components, chemical structure, and thermal stability as well as the micromorphology of the LFCC hydration products at high temps were analyzed from the micro point of view. Then, the modified leaf fiber's influence mechanism on the characteristics of LFCC at high temps was investigated.

## 2. Materials and methods

### 2.1. Materials

(1) Cement: 42.5R "Diamond" Brand ordinary Portland cement produced by Yanjiao New Building Materials Co., Ltd., Sanhe City, Hebei Province, China. The chemical composition of cement and mineral admixtures is shown in Table 1.

(2) Fly ash: II fly ash from Beijing Shijingshan Power Plant, China. The chemical composition of the fly ash is shown in Table 1.

(3) Leaf fibers: The leaves are poplar leaves (from now on referred to as leaves) collected from Beijing's downtown areas in November. The collected leaves were dried, crushed, screened, and processed into fibers (granules). The fiber size range was set to 0.3–1.18mm to increase the comparability. The screened leaf fibers were combined according to the mass ratio of 0.3 mm: 0.6 mm: 1.18 mm = 1:1:1. Figure 1 depicts the appearance and morphology of poplar leaves and fibers, while Table 2 depicts the chemical components of leaf fibers. Table 3 displays the bulk density and apparent density of leaf fibers with varying particle sizes.

(4) Polycarboxylic acid superplasticizer (PC): Purchased from Beijing Muhu Admixture Co. Ltd., China, PH = 8.5–9.5, solid content ≥97%, density 498.0 kg/$m^3$, water reduction rate >35%, and dosage 0.6%–1.3%.

(5) Calcium chloride ($CaCl_2$): Produced by Beijing Chemical Plant, China, density 2150 kg/$m^3$ and melting Point 782 °C.

(6) Triethanolamine ($N(CH_2CH_2OH)_3$): Produced by Beijing Chemical Plant, China, boiling point 360.0 °C, and melting point 21.2 °C.

(7) Water: Drinking water complied with China's national standards, pH = 6.91 at 25 °C.

(8) Pure acrylic polymer emulsion: PRIMAL MAC-261P acrylic polymer emulsion by Rohm and Haas, USA, density 1.04 g/ml, total solid content 50.0%.

(9) Water glass solution ($Na_2O{\cdot}nSiO_2$): Produced by Beijing Yongfei Adhesive Factory, China, modulus 3.1, Baumé scale 40°, density 1.38 g/ml, total solid content 36.20%.

(10) Flame retardant: Procured from Taixing Fine Chemical Co., Ltd., Jinan, Shandong Province, China. ①Ammonium polyphosphate (APP): The model is HT-208, $P_2O_5$ content ≥57.0%, and N content ≥12.0%, easily soluble in water, pH value 4.5–6.5. ②Magnesium hydroxide (MH): The model is HT-206, $Mg(OH)_2$ content ≥91.5%, molecular weight 58.3 and density 2.36 g/$cm^3$, loss of ignition ≥28%, pH value 9–11. ③Aluminum hydroxide (ATH): The model is HT-205, $Al_2O_3$ content ≥64.0%, molecular weight 78, and density 2.42 g/$cm^3$, loss of ignition 34.0%–35.0%, and pH 8.5–10.5.

### 2.2. Methods

(1) Determination of the maximum solubility of flame retardants

Three flame retardants, APP, MH, and ATH, were used to test the three flame retardants' maximum solubility at different water temperatures (the suspension that can be sprayed is enough) to facilitate the spray modification of leaf fibers. The results are shown in Table 4.

(2) Modification methods of leaf fibers

The fibers were pretreated with physical processes. First, the leaf surfaces were sprayed with a flame-retardant solution. When dried, we apply another flame-retardant solution, spraying it over the surface. Finally, in order to cover the fiber surfaces in a thin layer, acrylic polymer emulsion or sodium silicate solution was sprayed onto them. During the concrete mixing and molding procedure, flame retardants wrapped on the fiber can easily be lost into the cement, affecting the fibers' flame-retardant effect. The covering layer could prevent that by encasing and shielding the flame retardant. The modification method of leaf fiber is shown in Figure 2. The specific way is to smoothly spray the flame-retardant solution from the sprayer nozzle in a foggy form and achieve a uniform coating. The flame retardant to water dilution ratio was 1:1 (mass ratio). Before dilution, the following is the ratio of flame retardant to the mass of plant fibers: APP, MH, and ATH APP accounted for 60% of fiber mass, and before dilution, sodium silicate solution and acrylic

**Table 1.** Chemical composition of cement and mineral admixtures (wt.%).

| Type of materials | CaO | $SiO_2$ | $Al_2O_3$ | $Fe_2O_3$ | $TiO_2$ | MgO | $SO_3$ | $Na_2O$ | Ignition loss |
|---|---|---|---|---|---|---|---|---|---|
| Cement | 62. 38 | 25. 52 | 6. 15 | 3. 27 | 0. 57 | 1. 54 | 1. 65 | 0. 21 | 2. 87 |
| Fly ash | 1. 93 | 54. 88 | 32. 12 | 4. 28 | — | 1. 45 | 1. 46 | — | 3. 82 |


**Figure 1.** Appearance of poplar leaves and their fibers: (a) Poplar leaves; (b) Poplar leaves fibers.

**Table 2.** Chemical composition of leaf fibers (wt.%).

| Item | Moisture content | Ash content | Holo-cellulose | Cellulose | Pentosan | Lignin | Pectin | Extracts of different solutions | | | |
|---|---|---|---|---|---|---|---|---|---|---|---|
| | | | | | | | | Hot water | Cold water | Alcohol benzene | 1% NaOH |
| Leaf fibers | 5.15 | 13.15 | 50.78 | 25.48 | 10.44 | 23.00 | — | 33.51 | 28.31 | 21.44 | 38.54 |

**Note:** It is determined following China's national standard GB/T 2677 the Testing Methods of Relevant Components of Paper-making Materials. Holocellulose is the sum of cellulose and hemicellulose in raw materials of plant fibers, also known as full-cellulose.

**Table 3.** Bulk density and apparent density of leaf fibers with different particle sizes (kg/m$^3$).

| Particle size (mm) | 4.75 | 2.36 | 1.18 | 0.6 | 0.3 | 0.15 & below |
|---|---|---|---|---|---|---|
| Bulk density | 97.2 | 176.1 | 234.4 | 280.3 | 282.1 | 302.2 |
| Apparent density | 224.6 | 306.7 | 336.8 | 357.1 | 295.4 | 297.5 |

Note: The sieving of leaf fibers with different particle sizes and the bulk density tests were carried out in accordance with China's national standard GB/T14684-2001 (Building sand).

**Table 4.** Maximum solubility of flame retardants (g/100g water).

| Type | 20 ± 0.5 (°C) | 40 ± 0.5 (°C) | 60 ± 0.5 (°C) |
|---|---|---|---|
| APP | 40 | 50 | 60 |
| MH | 30 | 40 | 50 |
| ATH | 30 | 40 | 50 |

polymer emulsion accounted for 42% of the fiber mass. The sprayed fibers were placed into an electric blast and dried at 85 ± 1 °C for 24–30 h. They were cooled at room temperature and put in sealed plastic bags for future use when reaching the dried state.

(3) Mixing ratio of LFCC

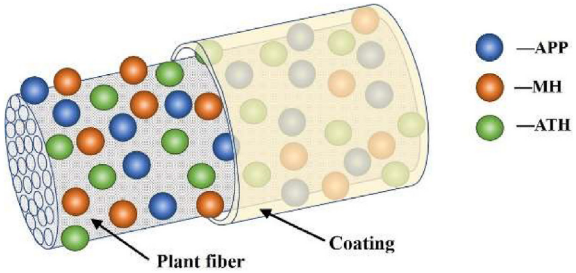


**Figure 2.** Sketch map of modification method of leaf fibers.

Table 5 displays the LFCC mix proportion. In order to properly mix, the mixture's consistency should be regulated at 30±3mm, and the adjustments to water consumption should be made accordingly [14].

(4) Fabrication of LFCC mechanical property specimens

Related work was carried out according to GB/T17671-1999 [15]. The size of samples was 40 mm × 40 mm × 160mm, and standard curing was 28d. From each group, we selected three specimens, dried, numbered, and weighed them; their mean strength was used to determine the test result for this group.

(5) Test of LFCC insulation performance

Relevant tests are carried out as described in GB/T10294-2008 [16]. SSX-DR300 intelligent Double Plate Thermal Conductivity Tester (by Shaoxing City, China) was used to measure thermal conductivity. The hot-plate temperature was set to 50 °C and the cold-plate temperature at 30 °C. The mix proportion of the specimens was the same as that of the mechanical property test specimens. The size of the samples was 300 mm × 300 mm × 30mm. At a temperature of 85 °C, we dried the samples for 24–30h before the test after 28 days of conventional curing. Two plate specimens from each group were tested for their thermal conductivity. LCFF's eventual assessment of their thermal insulation performance depended on the mean of the test results of two specimens.

(6) Performance test of LFCC at high temperatures

We conduct LFCC high-temperature heating experiments using a box-type resistance furnace. The specimens in the furnace are shown in Figure 3. Set the heating rate to 10 °C/min, and set the test temperature to 25 °C, 150 °C, 250 °C, 350 °C, 500 °C, and 650 °C. The furnace will

**Table 5.** Mix ratio of LFCC (kg/m$^3$).

| Cement | Fly ash | Leaf fibers | Total water consumption | PC | $CaCl_2$ | $N(CH_2CH_2OH)_3$ |
|---|---|---|---|---|---|---|
| 668.25 | 74.25 | 111.28 | 360 | 5.94 | 14.85 | 0.74 |

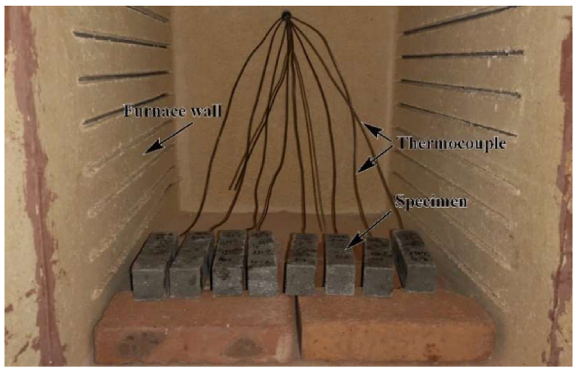


**Figure 3.** LFCC specimens in furnace.

continue to heat until it reaches the previously set temperature; it will keep heating at the constant temperature for an hour; and then the furnace door will be opened to allow the specimens to cool. The samples were cooled to room temperature for other performance tests.

(7) Thermal stability analysis of leaf fibers and flame retardants

Hitachi STA7300 Thermogravimetric Analyzer analyzed the thermal stability of the samples. Weigh 5–10 mg of the samples and put them into the crucible. With the protection of nitrogen, we set the heating rate to 10 °C/min, and the heating range was set to 30°C–1000 °C The weight loss/weight loss rate (TG/DTG) curve was chosen as the test mode.

(8) Analysis of the flammability of leaf fibers

The Limiting Oxygen Index (LOI) is used to evaluate materials' combustion properties [17]. The flammability of modified leaf fibers was evaluated using the JF-3 oxygen index tester. The determination method was carried out regarding GB/T2406.2–2009 [18] and GB/T 5454–1997 [19]. Sample preparation: The leaf fibers were inserted into a Φ10 mm × 120 mm paper tube, and the sample's fibers were made homogeneous and solid by compacting it with a thin wooden rod. For each modification scheme, five samples were chosen, and the average LOI of the five pieces was used as the outcome. Figure 4 shows the LOI test specimens and instruments.

(9) Chemical structure analysis of flame retardant and leaf fibers

A Tensor 27 Fourier Transform Infrared Spectrometer (FTIR) by Bruker, Germany, was used to analyze the chemical structure of the flame retardants and the leaf fibers. The scanning wavenumber range was set to 4000-400 cm-1, scanning times 32 times, and resolution 4cm$^{-1}$. The sample was made by mixing KBr and test materials into a semi-transparent ingot tablet. Way to prepare samples: 3.5mg test materials and a homogeneous transparent ingot tablet was obtained by pouring 300 mg of the 350 mg of KBr that had been added to the agate mortar, mingled, and ground into a pressing die pressed for 1–2 min, under pressure of around 10 MPa.

(10) Analysis of micro-morphology of leaf fibers and their LFCC

The micro-morphology of leaf fibers and their LFCC were examined using a Carl Zeiss NTS, Germany, SIGMA Thermal Field Emission Scanning Electron Microscope (SEM). In addition, the chemical composition of the leaf fiber microzones was examined using an X-MAX-20 X-ray Energy Dispersive Spectrometer (EDS) by Oxford, the UK, linked to a scanning electron microscope. We set the test voltage to 2 kV when we observe the leaf fiber. First, we dry the samples at 75 ± 1 °C and then sparge gold onto them for 30 s before testing. When watching LFCC, the test voltage was 10Kv. The same 28-day-old specimens used in the mechanical properties test were dried at 85 ± 1 °C, broken into 2mm-square pieces, and then sprayed with gold for half a minute.

(11) Modification scheme of leaf fibers

Table 6 displays the modification scheme for the leaf fibers. Corresponding to the serial numbers of each project in Table 6, in the following, the specimen marks of the leaf fiber performance test are Y0~Y7, and the specimen marks of the LFCC performance test are YC-1~YC-7.

## 3. Results and discussion

### 3.1. Chemical structure of flame retardants and leaf fibers

The chemical structure and functional groups of flame retardants and leaf fibers can alter, and this can be detected using Fourier Infrared Spectroscopy (FTIR). The FTIR spectra of flame retardants and leaf fibers are shown in Figures 5 and 6, respectively.

As shown in Figure 5, APP has an antisymmetric stretching vibration peak of NH4+ at 3431 cm-1, N–H stretching vibration peak of ammonium polyphosphate at 3242 cm-1, and N–H bending vibration peak at 1668 cm-1, P=O stretching vibration peak at 1290 cm-1. 1115cm-1 is the asymmetric stretching peak of the P–O bond, and 916cm-1 is the symmetric stretching peak of the P–O bond of ammonium polyphosphate [20, 21]. The stretching vibration peak of Mg–OH is denoted as MH. at 3705 cm-1 and O–H and Mg–OH bending vibration peaks at 1634 cm-1 and 1437 cm-1, respectively [22, 23, 24]. Adsorbed water and the –OH

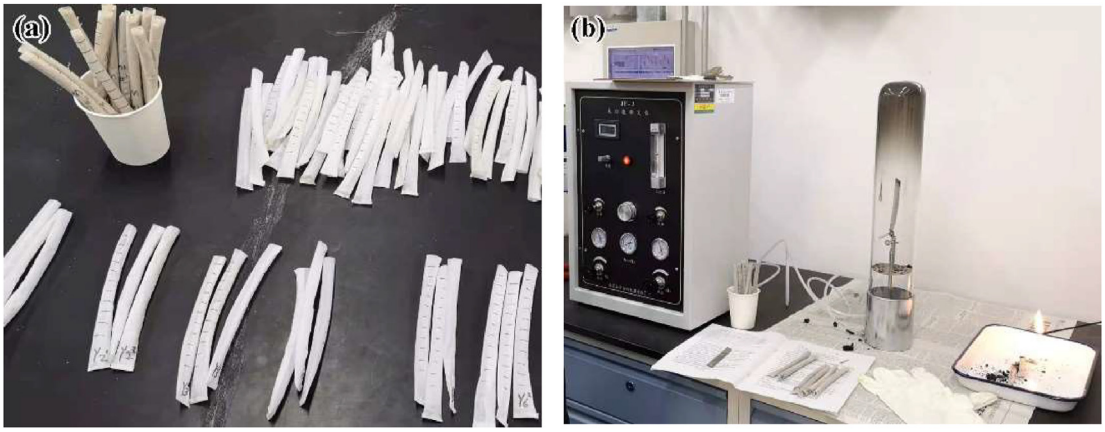


**Figure 4.** LOI test specimens and instruments: (a) specimens; (b) instruments.

**Table 6.** Modification scheme of leaf fibers.

| No. | Scheme |
|---|---|
| 0 | No treatment |
| 1 | Non-flame retardant →Pure acrylic |
| 2 | APP→ Pure acrylic |
| 3 | APP + MH→ Pure acrylic |
| 4 | APP + MH + ATH→ Pure acrylic |
| 5 | APP + MH×0.7 + ATH (replacing 30%MH)→Pure acrylic |
| 6 | APP + MH×0.5 + ATH (replacing 50%MH)→Pure acrylic |
| 7 | APP + MH×0.5 + ATH (replacing 50%HM)→Water glass |

group's stretching vibration may be superimposed at the absorption peaks at 3622 cm-1 and 3549 cm-1 in ATH, The $CO_2$ deformation vibration has an absorption peak at 2361 $cm^{-1}$. The absorption peak at 1628 cm-1 is the deformation vibration of adsorbed water. At 1396 cm-1, the absorption peak corresponds to the OH group's in-plane bending vibration, at 1020 cm-1, 968 cm-1, and 914 c cm-1, and at 667 cm-1, the absorption peak corresponds to the stretching vibration of the Al–O group [25].

In Figure 6(a), comparing Y1 with Y0, the pure acrylic emulsion film acts on the surface of the leaf fibers through a blue shift at 3447 $cm^{-1}$, the appearance of the absorption peak at 2957 $cm^{-1}$, and the enhancement of the peak value at 1743 $cm^{-1}$, and the like. APP in Y2 increases the absorption peak of hydroxyl stretching vibration by $NH_4^+$ at 3443 $cm^{-1}$ and increases the absorption peak value of hydroxyl stretching vibration by 1269 and 1269 in Y2. Moreover, the P=O stretching vibration peak of ammonium polyphosphate at 3699 $cm^{-1}$ acts on the surface of leaf fibers; MH in Y3 is successfully adsorbed on leaf fibers' surface with the appearance of free OH stretching vibration characteristic band at 3699 $cm^{-1}$ to modify them [26, 27, 28, 29].

In Figure 6(b), it can be seen that ATH in Y4 acts on the surface of leaf fibers through the superposition effect of the characteristic bands of stretching vibration of free –OH in ATH at 3524 cm-1 and the stretching vibration at 667 cm-1 of Al–O in ATH. In comparison to Y3, in Y5 and y6, the stretching vibration peak of the free –OH group of MH at 3699 cm-1 gets blurrier as the rate at which ATH replaces MH increases, and the corresponding deformation vibration peak of –OH at 1024 cm-1 and Al–O corresponding stretching vibration peak at 667 cm-1 becomes more evident, indicating that the substitution of MH by ATH affects the chemical structure. When Y7 was compared to Y6, the C=O bond stretching vibration absorption peak of ethyl acrylate (EA) molecules at 1743 cm-1 vanished, and characteristic Si–O–Si stretching vibration peaks in sodium silicate appeared at 1090 cm-1 and 469 cm-1. These

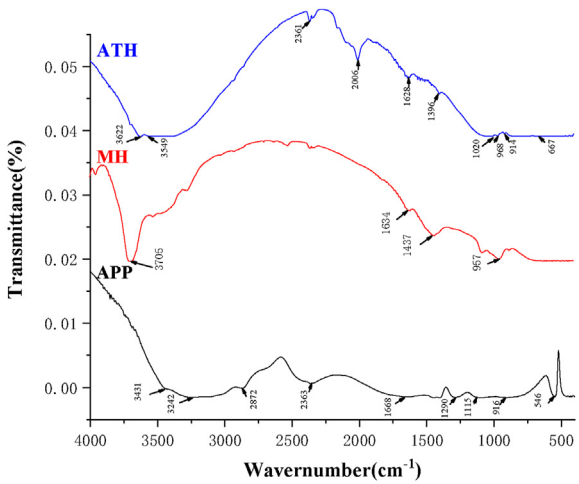


**Figure 5.** FTIR spectra of three flame retardants.

results show that the sodium silicate coating was successful in acting on the exterior of leaf fibers [30, 31].

As shown in Figure 6, the flame-retardant modifiers and the exterior coating have an impact on chemical groups of leaf fibers. Thus, the change in chemical structure is bound to influence leaf fibers' thermal stability, flammability, and physical and mechanical properties.

### 3.2. Thermal stability of flame retardants and leaf fibers

#### 3.2.1. Thermal stability of flame retardants

The TG/DTG analysis results of APP, MH, and ATH [32, 33, 34, 35] are shown in Figure 7. As shown in Figure 7(a), the thermal decomposition of APP can be roughly divided into three stages. The volatilization of a minor quantity of adsorbed water was mostly responsible for the first stage, which ranged from 30 °C to 182.6 °C. The second stage, from 182.6 °C to 542.9 °C, primarily generated ammonia and water vapor, and the product was polyphosphoric acid. In the third stage, from 542.9 °C to 1000 °C, the weight loss was mostly brought on by the generation of phosphorus oxides produced by the continued oxidation of polyphosphoric acid (To create P–O molecules, polyphosphate consumed $H_2O$).

As shown in Figure 7(b), the thermal decomposition of MH can be roughly divided into two stages: the first stage was 30–428.1 °C, mostly brought on by the absorbed water's release and the majority of the brucite's. Brucite was transformed into periclase. The second stage was 428.1–701.5 °C, mainly caused by escaping residual crystal water from brucite and the transformation into magnesium oxide.

The thermal degradation of MH could be generally separated into two phases, as illustrated in Figure 7(b). The first stage was from 30 °C to 274.9 °C, mainly the adsorption of water volatilization and partial dropout of OH from the gibbsite. The second stage was from 274.9 °C to 314.6 °C, Al $(OH)_3$ was severely dehydrated at this stage, and most of the OH was dropped out from the gibbsite and converted into diaspore AlO(OH). The third stage was from 314.6 °C to 558.3 °C, mainly the dropout of gibbsite OH, transforming into $Al_2O_3$.

#### 3.2.2. Thermal stability of leaf fibers

Figure 8 displays the results of the TG/DTG analysis of leaf fibers [36, 37, 38, 39], and Figure 9 displays the residual weight rate of Y0–Y7 after pyrolysis at 1000 degree centigrade.

Figure 8(a), the pyrolysis process of Y0 leaf fibers can be broadly separated into three phases three stages: the first stage was from 30.0 °C to about 131.91 °C. Free water evaporation and the combined water's dehydration reaction in the leaf fiber caused this stage, which belongs to the stage of dehydration and drying. The second stage, from 131.91 °C to 471.14 °C, was the pyrolyzation stage of holocellulose. The spot at 268.75 °C should be where maximum pyrolyzation of hemicelluloses occurs. Because of the irregular amorphous structure of hemicelluloses, they have low thermal stability. At 331.45 °C, The maximum weight loss rate peak appeared, which, being cellulose pyrolysis, released much heat. D-glucose linked to a glycoside bond forms a macromolecular structure known as cellulose. It has no branches and is challenging to decompose; the weight loss rate at this stage was 54.63%. In the third stage, from 471.14 °C to 1000 °C, there are two prominent weight loss rate peaks at 484.34 °C and 656.51 °C, respectively. Because lignin's primary constituent, a polysaccharide made of phenylpropane joined by an ether and carbon bond, has a high degree of stability and is challenging to break down. This stage should be the pyrolysis of lignin.

Comparing Figure 8(b) with Figure 8(a), the DTG curve shows a sharp peak in the weight loss rate of Y1 at 386.44 °C, that was because in pure acrylic polymer emulsions, the macromolecular polymer could decompose at such a temperature [40].

Comparing Figure 8(c) with Figure 8(b), the DTG curve had two more weight loss rate peaks at 202.30 °C and 899.47 °C, which were caused by the thermal decomposition of APP on the surface of leaf fibers. APP produced ammonia and water vapor at 202.30 °C, the product being

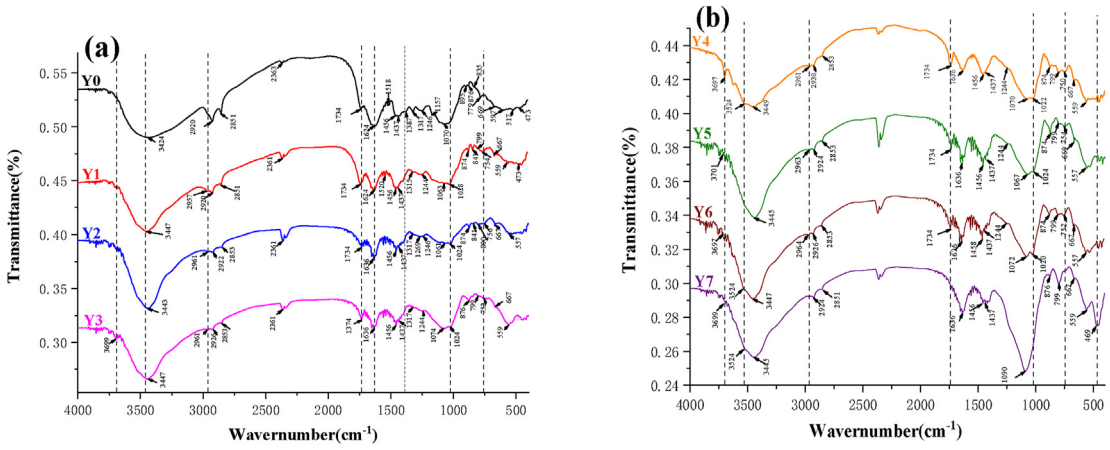


**Figure 6.** FTIR spectra of leaf fibers: (a) Y0~Y3; (b) Y4~Y7.

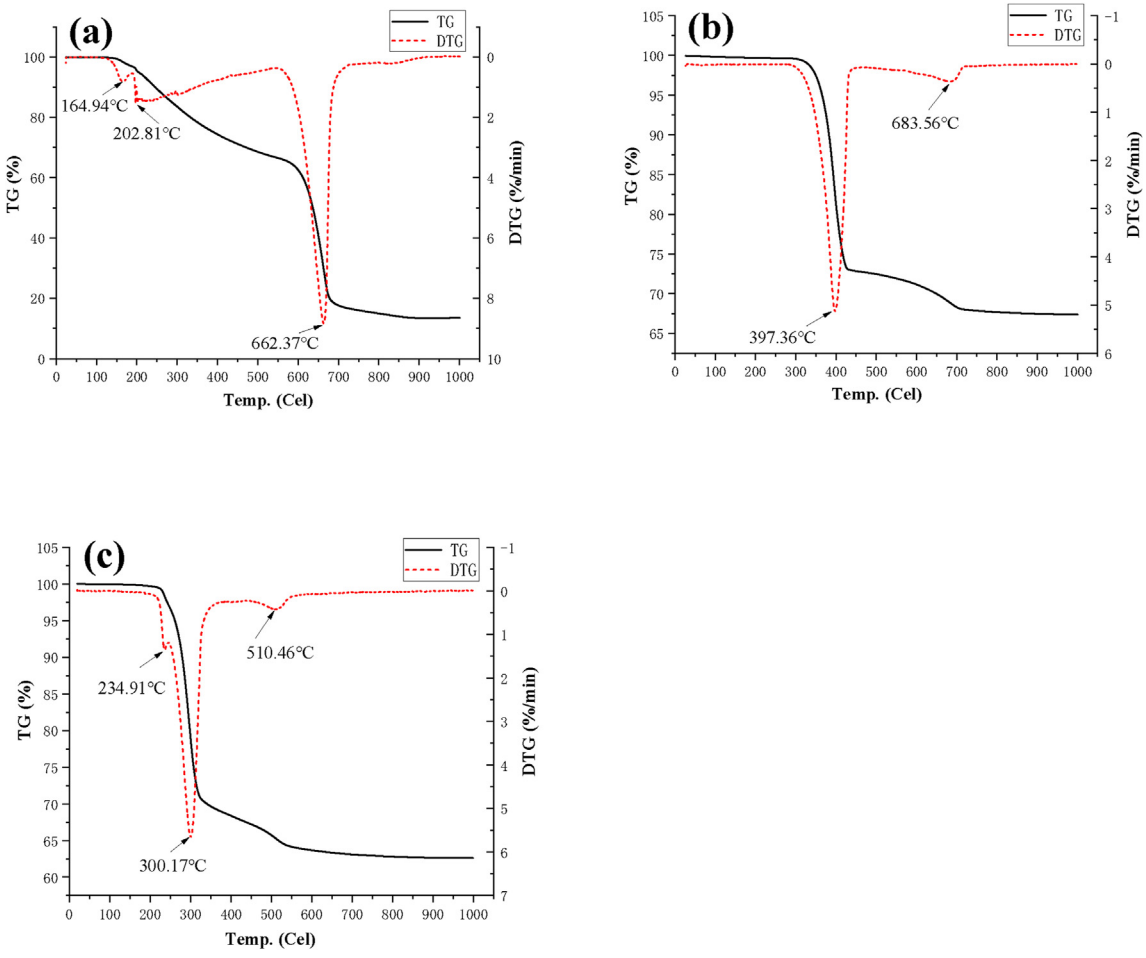


**Figure 7.** TG/DTG analysis of three flame retardants: (a) APP; (b) MH; (c) ATH.

polyphosphoric acid. The polyphosphoric acid underwent additional oxidation at 899.47 °C to produce phosphorus oxide. The TG curves show that, because of APP's flame retardancy, the total weight loss of Y2 decreases in the temperature range from 30 °C to 1000 °C, demonstrating a significant improvement in Y2's thermal stability.

Comparing Figure 8(d) with Figure 8(c), the peak maximum weight loss rate in Figure 8(d) appeared at 111.65 °C, which was caused by free water volatilization and combined hydrolysis adsorption dehydration of leaf fiber and flame retardants. Due to MH flame retardant addition, the maximum rate of weight loss rate at this drying stage is significantly higher than that of Y2 and is 54.65 °C later than Y2. At 286.57 °C and 331.84 °C, the maximum weight loss rate peaks of hemicellulose and cellulose were observed. The temperature of the two peaks was later compared to Y2 due to the synergistic effect of MH. The maximum rate of weight loss peak appeared at 395.29 °C, resulting from the breakdown of macromolecular polymer in pure acrylic polymer emulsion. Under the co-action of APP and MH, the temperature was delayed by 4.10 °C than Y2.

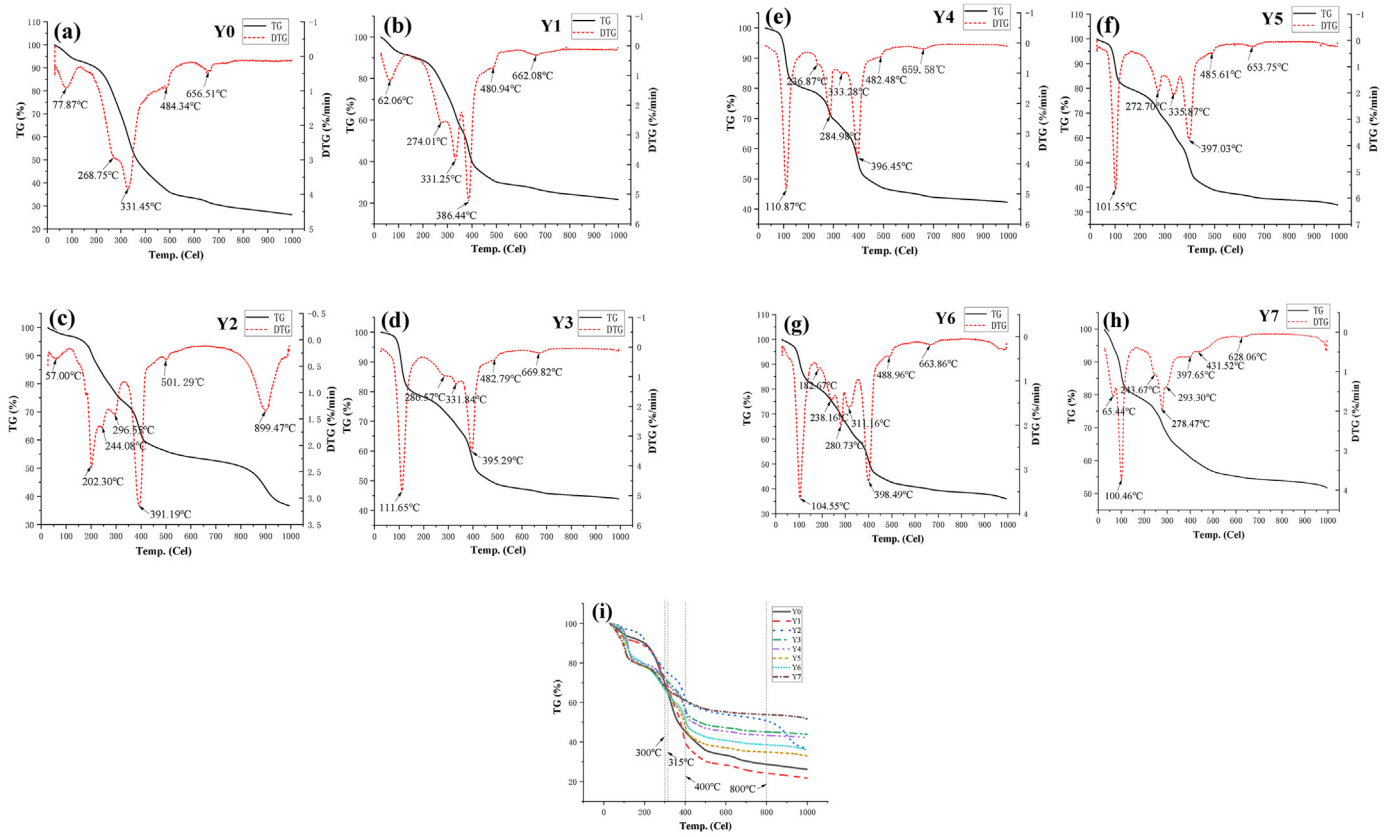


**Figure 8.** TG/DTG analysis results of leaf fibers: (a)~(h) correspond to samples Y0~Y7 respectively; (i) TG curves of samples Y0~Y7.

Comparing Figure 8(e) with Figure 8(d), it can be seen on the DTG curve that most peaks appeared at 236.87 °C, which was caused by partial loss of OH out of ATH.

Comparing Fig. (f) with Figure 8(e), it is clear that, because of the decreased ATH content, in Figure 8(f), there is no weight loss rate peak on the DTG curve.

Under the combined action of MH and ATH, APP produced a portion of water vapor and ammonia, as shown by the DTG curve in Figure 8(g) at 182.67 °C, and the end product was polyphosphoric acid. At238.16 °C, the partial loss of OH out of ATH was the reason.

Comparing Figure 8(h) with Figure 8(g), because Y7 used sodium silicate as its fiber coating, it has no peak of the macromolecular polymer's decomposition weight loss rate in the pure acrylic polymer emulsion. Y7 leaf fibers' pyrolysis could be generally separated into three stages: the first stage is from 30 °C to 165.42 °C, and the weightless rate peaks appeared at 65.44 °C and 100.46 °C, due to free water evaporation and bound water desorption of leaf fiber, and the application of flame retardants. belonging to the drying stage. The second stage is from 165.42 °C to 352.15 °C, and the weight loss rate peak at 243.67 °C, which was caused by partial OH removal from ATH. At 278.47 °C and 293.30 °C, the peaks are of hemicelluloses and celluloses' maximum weight loss rate peaks. The third stage is from 352.15 °C to 996.37 °C, the peak of the weight loss rate at 397.65 °C, which was caused by the partial water loss of MH. The decomposition caused by high temperatures of some lignin and complex polymer compounds led to the weight loss rate peaks at 431.52 °C and 628.06 °C.

Generally, the higher the high-temperature residual weight rate of the material, the better its thermal stability [41]. Fibers that have not had flame retardant treated Y0 & Y1 are demonstrated in Figures 8 and 9 to be relatively constant at the low-temperature stage. nonetheless, the mass loss decreased significantly after 300 °C. Because Y1 is covered in a pure acrylic emulsion organic coating layer, its fibers have increased flammability, making its fiber thermal stability worse than Y0. The thermal stability of Y2 at medium and low temperatures is satisfactory, however the weight loss rate decreased distinctly when the temperature was above 800 °C. The mass-loss rate of Y3 and Y4 modified with composite flame retardant is less after 800 °C, and the residual weight rates of the two at 1000 °C are 43.91% and 42.27%, respectively, and the thermal stability of the two is excellent. The thermal stability of Y6 is better than that of Y5. After 315 °C, the thermal stability of Y5 and Y6 is worse than that of Y3 and Y4. Y7 exhibited the largest residual weight rate, the less mass loss rate, and the best thermal stability when the temperature exceeded 400 °C. The presence of the water-glass layer increases the retention rate of flame retardants in the fibers, and the thermal stability as well as their flame retardancy are also improved. The sodium silicate inorganic has good high-temperature stability before 1200 °C [42].

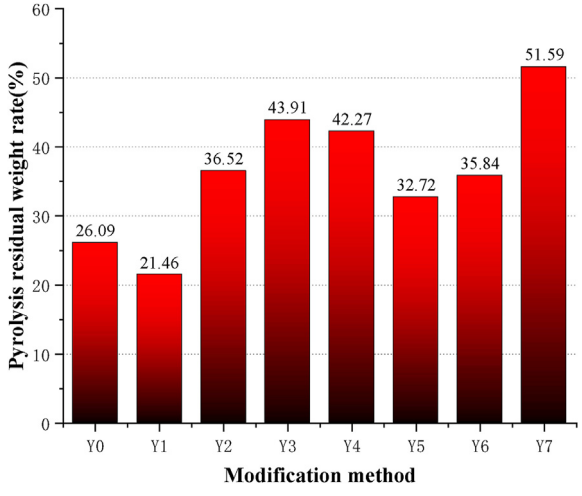


**Figure 9.** Pyrolysis residual weight rate of leaf fibers.

In short, the ones with satisfactory thermal stability are Y7, Y3, Y4, Y2, Y6, and Y5, and the ones with poor thermal stability are Y1 and Y0.

### 3.3. Flammability of leaf fibers

If a material is non-flammable, that means its LOI is high. In contrast, If a material is combustible, that means its LOI is low [43]. The material with less than 22.0% LOI is generally considered flammable, the material with LOI between 22.0% and 27.0% is flammable, and the material with an LOI greater than 27.0% is considered nonflammable [44, 45]. The LOI results of leaf fibers are shown in Figure 10.

As shown in Figure 10, the LOI of Y0 is 23.0%, meaning a flammable material. The LOI of Y1 coated with pure acrylic emulsion is 2.0% lower than Y0, indicating that leaf fibers' flammability is increased by pure acrylic emulsion organic compound. When Y2–Y7 was treated with a flame retardant, the LOI was greater compared to when it wasn't. Because of App, In Y2–Y6, the LOI of Y2 was higher,a flame retardant with good properties, is water soluble. Spray modification APP has good retention in fibers due to its ease of penetration and equal distribution. However, the composite flame-retardant modified fibers, resulting from a process of stirring and drying, suffered inevitable damage and uneven distribution of inorganic flame-retardant agents on the fiber surfaces, and the flame-retardant effect was affected. The LOI of Y5 and Y6 dropped by 2.2% and 2.5%, respectively, as compared to Y3, showing that the flame retardancy of leaf fibers was not enhanced when 30% and 50% of MH fibers were substituted by ATH. Compared to Y6, LOI for Y7 is 11.5% greater. The sodium silicate coating has a flawless flame-retardant impact on the leaf fibers due to its good thermal stability and adhesion, which helps sustain flame retardant retention on the fibers' surface.

### 3.4. Micro-morphology and chemical composition of leaf fibers

Figure 11 depicts the EDS test region and the micro-morphology of leaf fibers, and Figure 12 displays the test findings for the chemical composition of the test area. Interpretation of spectrum test processing: The K-line system has been used to normalize all of the evaluated items.

As shown in Figure 11, there are raised pores and granular debris on the surface of Y0, which, being prone to peel-off, will make fibers more permeable to water, which will alter how well fibers adhere to cement-based surfaces. There is also a smooth wax layer and cuticle layer on the surface of Y0, which is disadvantageous to the wetting, diffusion, and permeation of cement slurry and various additive solutions on the surface of fibers affecting the bonding between fibers and cement-based materials [2]. The pure acrylic emulsion film on the surface of Y1 fiber covered the detritus. It reduced surface flaws and improved the integrity of fibers by filling holes and fissures on their surface. The existence of polymer film improved the water resistance and alkali corrosion resistance of fibers, reduced the effect of the extracts in fibers on the anti-coagulation of cement hydration, and improved the interface effect between the fiber surfaces and the cement-base materials, thus increasing the bond between them. However, because the Y2 fibers were modified with APP flame retardant, they had to undergo spraying and dry processes that Y1 did not need, making them suffer more serious surface damage than Y1 fibers and reducing the coating uniformity of polymer film. Similarly, in Y3–Y7, adopting inorganic flame retardants MH and ATH required additional processes, making different sizes of fiber chips and flame-retardant agglomerated particles bonded on the surface, resulting in increased fiber surface defects and the deterioration of coating uniformity. As a result, the flame retardant is somewhat lost, and the binding strength among leaf fibers and cement mortar is affected. Comparing Y7 with Y6, the particles bonded on Y7 surfaces appeared loose and brittle. In contrast, the particles bonded on Y6 surfaces are increasingly hardened and flexible. That is because of the different characteristics of two organic and inorganic coatings made of pure acrylic emulsion and sodium silicate solution.

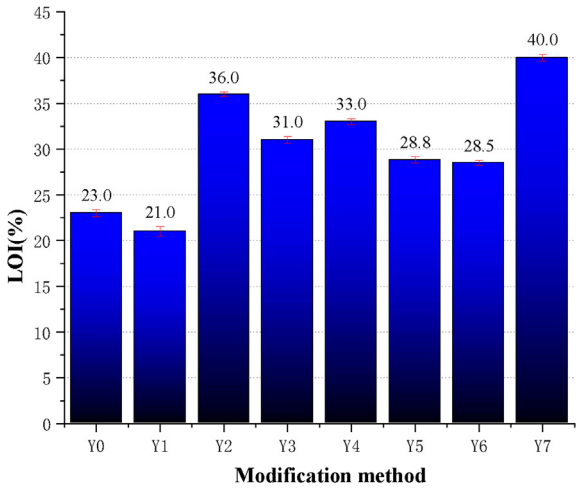


**Figure 10.** LOI of leaf fibers.

Elements C, O, and Si are mostly present on the exterior of untreated leaf fibers Y0, as illustrated in Figure 12 (The energy spectrum cannot be used to detect the single electron that exists outside of the nucleus of hydrogen). So, the majority of the leaf fibers are made of organic materials like C, H, and O, with a trace quantity of ash like SiO2 on the exterior cuticle. On the surface of Y1, there are mainly C and O elements, but no apparent Si elements were found caused by the effect of pure acrylic emulsion coating. The fact that P is present in Y2 shows that the APP flame retardant has well attached to the exterior of fibers. Since MH flame retardant was effectively deposited on the exterior of fibers, Y3 contains more Mg elements than Y2. Y4 has more Al than Y3, indicating that the ATH flame retardant has successfully adsorbed on the surface of fibers. Three flame retardants, P, Mg, and Al, were found in Y5–Y7. Using sodium silicate as a coating layer, Y7 mainly contains Na2O·nSiO2. As a result, Si and Na elements were discovered in the fibers, and the peak strength of the Si element was higher than that in Y0.

### 3.5. Performance of LFCC at high temperatures

#### 3.5.1. The mass-loss rate of LFCC at high temperatures

Figure 13 displays the mass-loss rate of LFCC at high temperatures. As shown in Figure 13, YC-7 has the highest mass loss rate of LFCC at high temperatures, of which mass-loss rates are 18.89% at 650 °C, followed by YC-1 and YC-2, of which mass-loss rates are 16.09% and 13.68%, respectively, at 650 °C. YC-4 has the lowest mass-loss rate, followed by YC-3, of which mass-loss rates are 10.26% and 10.93%, respectively, at 650 °C. The mass-loss rate is correlated with water volatilization in concrete, fiber plants', and flame retardants' heat release of water, gas, etc. The thermal stability of composite flame-retardant treated fibers LFCC (except YC-7) is higher than that of fibers treated with no flame retardant and sole component flame-retardant treated fibers LFCC. Hence, their LFCC mass-loss rate is relatively low. Since the YC-7's inorganic coating of sodium silicate is brittle and hard, it will inevitably crack in the LFCC mixing process (see Figure 17). The LFCC will experience high heat mass loss as a result of loss of flame retardants or the uneven distribution, which causes poor flame retardancy of fibers.

#### 3.5.2. Strength of LFCC at high temperatures

*3.5.2.1. Compression strength of LFCC at high temperatures.* The compressive strength and loss rate of LFCC at high temperatures are shown in Figure 14.

As shown in Figure 14(a), the compression strength of LFCC decreased with the increase in temperature, especially from 500 °C to 650 °C. LFCC suffered significant strength attenuation. At 650 °C, YC-7

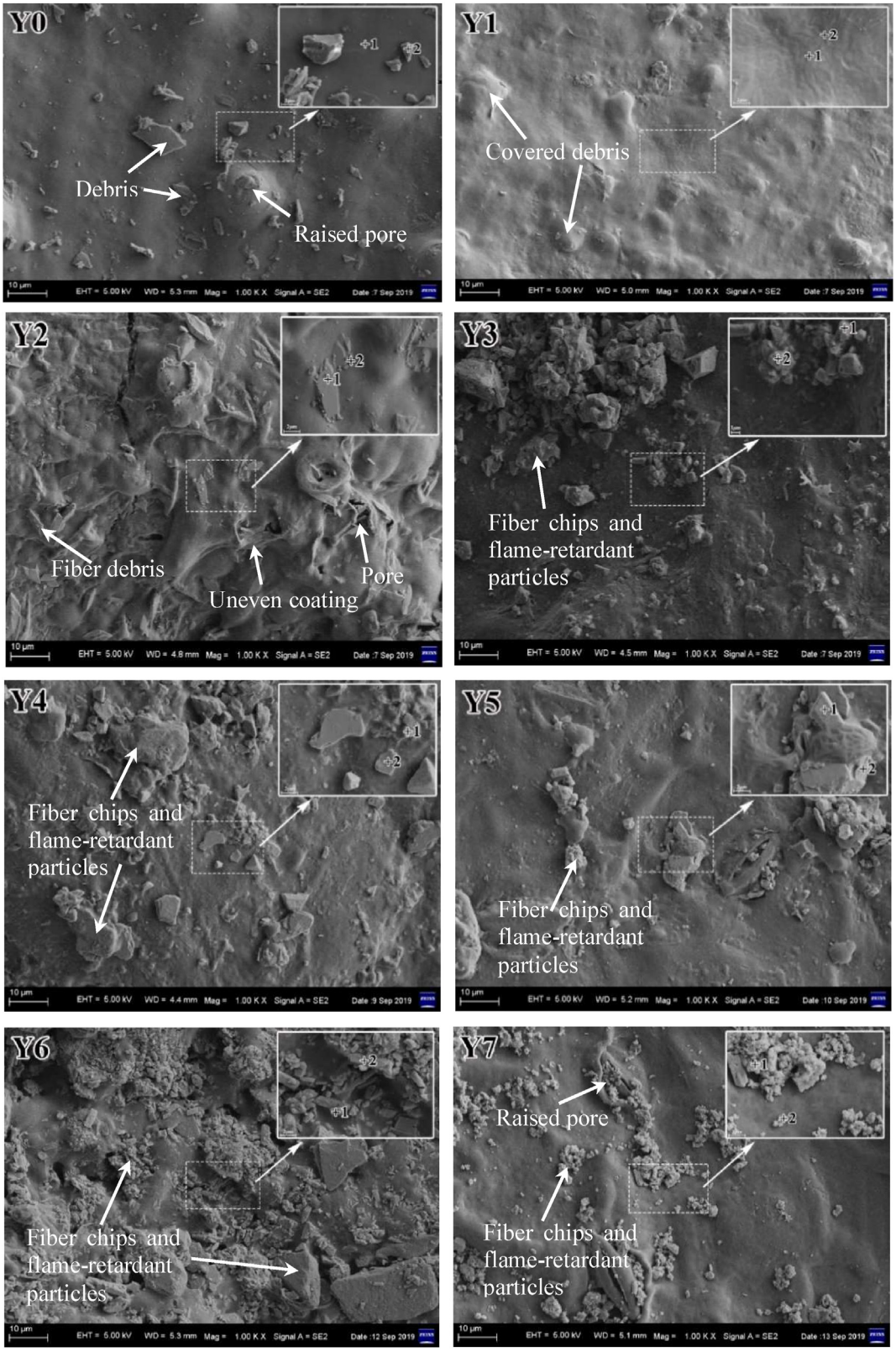


**Figure 11.** Micro-morphology and test area of leaf fibers (1000 times): Y0~Y7 correspond to the serial numbers in Table 6.

had the highest compression strength (5.13 MPa), followed by YC-6 (3.60 MPa) and YC-5 (3.10 MPa). At 650 °C, YC-1 had the lowest compression strength (0.33 MPa), followed by YC-2 (0.62 MP A). The strength of YC-2 to YC-5 samples increased during the heating process, which is related to the rate of hydrate formation being more significant than that of hydrate pyrolysis, and the incomplete pyrolysis of plant fibers could provide certain tensile strength for cement matrix. There are the main reasons for the decrease in LFCC compression strength at high temperatures: Firstly, the temperature stress will cause the occurrence and expansion of micro-cracks in the cement matrix. Secondly, the dehydration and

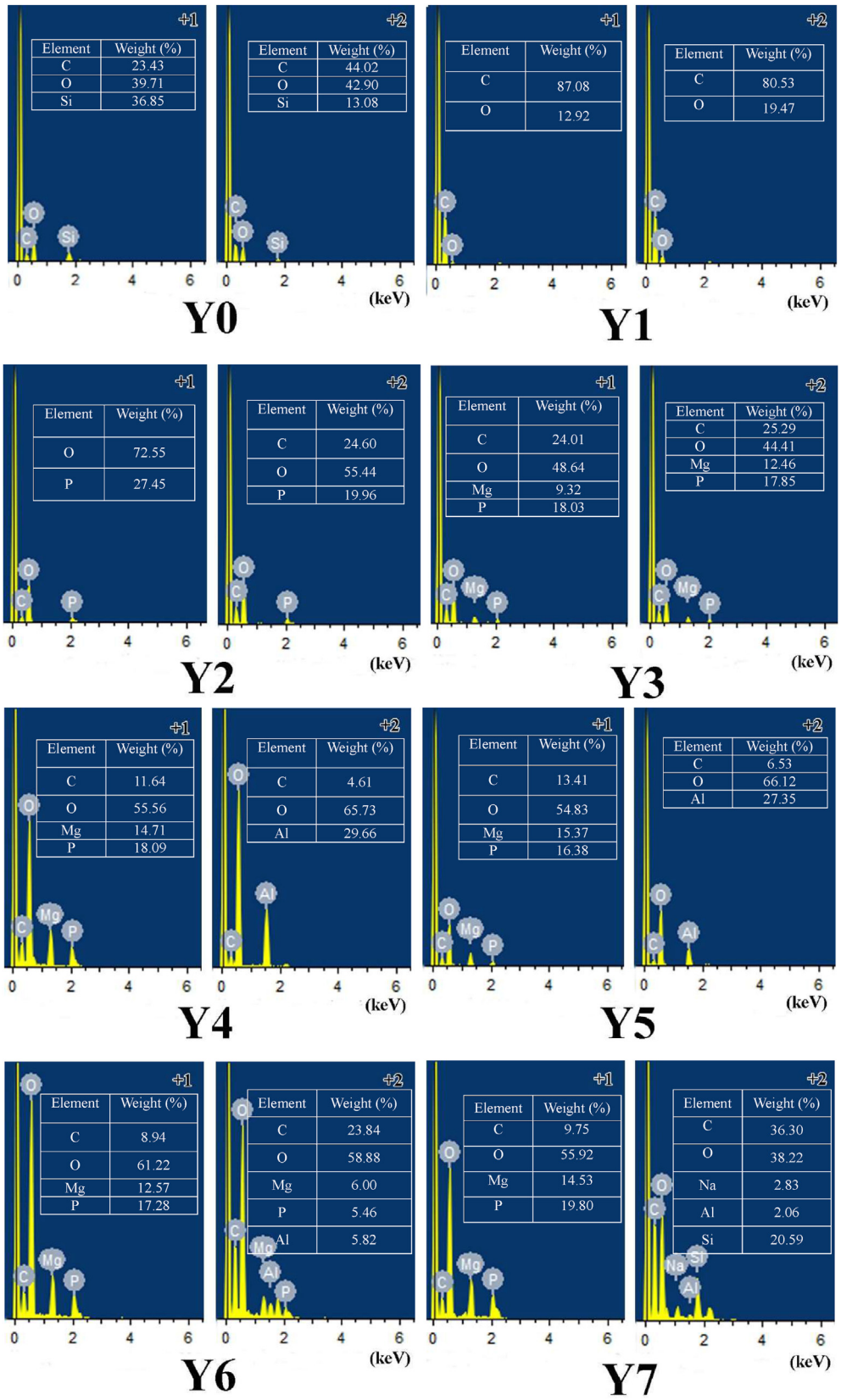


**Figure 12.** Chemical composition of leaf fibers in EDS test area.

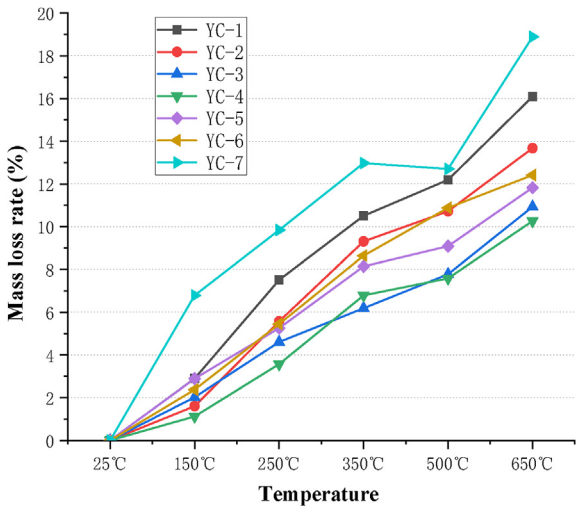


**Figure 13.** Mass-loss rate of LFCC at high temperatures.

decomposition of hydration products, e.g., hydrated calcium sulphoaluminate (Aft), will thermally decompose at 200 °C, $Ca(OH)_2$ begins to dehydrate at 400 °C, while C–S–H gel and $CaCO_3$ start to decompose at over 600 °C [46]. And thirdly, the enhanced crack resistance provided for cement matrix by thermal decomposition of fiber plants will reduce to some extent.

Figure 14(b) shows that at 650 °C, YC-1 and YC-2 have the most significant loss rates of LFCC compression strength, which are 95.15% and 83.56%, respectively. YC-3 and YC-4 have the lowest loss rates of compression strength, which are 38.27% and 54.01%, respectively. While YC-5, YC-6, and YC-7 have an approximately similar loss rate of compression strength. According to the results, composite flame-retardant fibers improve the thermal stability of LFCC more than non-flame-retardant fibers or single flame-retardant fibers. Hence the loss rate of LFCC compression strength is relatively low.

*3.5.2.2. Flexural strength of LFCC at high temperatures.* Figure 15 displays the flexural strength and loss rate of LFCC at high temperatures.

As shown in Figure 15(a), as the temperature rises, the flexural strength of LFCC typically declines, which could be generally split into three stages: 25°C–150 °C, the strength decrease amplitude is relatively small, and some even increase; the second stage: 150°C–350 °C, the strength decrease amplitude is relatively large, especially at 150°C–250 °C, the strength will decrease sharply; the third stage: 350°C–650 °C, the strength decrease amplitude is relatively small but stable. At 650 °C, YC-5 and YC-6 have high flexural strength, 0.90MPa, and 0.79MPa, respectively, while YC-3 has low flexural strength, 0.20MPa. The same factor that causes LFCC's flexural strength to drop at high temperatures also accounts for its compression strength.

It can be seen from Figure 15(b) that, on the whole, the flexural strength loss rate of LFCC increases with the increase in temperature. The flexural strength loss rate of LFCC increases slowly in the range of 25°C–150 °C and even increases in YC-3. This is because the damage made by temperature to the sample's structure is less than the repair degree made by hydrate growth to the structure [47]. At 650 °C, YC-6 has a small flexural strength loss rate, 74.74%, followed by YC-2 and YC-8, 75.22% and 75.54%, respectively. YC-1 has the largest flexural strength loss rate, 88.73%, followed by YC-3 and YC-9, of which loss rates are 85.80% and 85.78%, respectively.

In short, based on the examination of mass loss rate and mechanical properties presented above, the LFCC with better fiber modification effect is YC-5 and YC-6, followed by YC-4, YC-3, and YC-7, and the LFCC with poor fiber modification effect is YC-1 and YC-2. It shows an optimal match issue between LFCC's mechanical and physical properties at high temps and procedures used to modify leaf fibers for flame retardancy. The thermal stability of leaf fibers and the bonding strength between flame-retardant fibers and cement-base materials are both factors that affect LFCC strength at high temperatures. Among the fiber modifiers YC-5 and YC-6, the substitution of MH by ATH is 30% and 50%, respectively. The three composite flame retardants work well together to improve the thermal stability of the fibers while also preventing cement matrix from containing excessive amounts of MH and ATH filler, which has little impact on the processing and mechanical characteristics of the cement-base materials [48]. As a result, the strength loss and mass loss of LFCC are relatively minor.

*3.5.3. Thermal insulation performance of LFCC at high temperatures*

Figure 16 displays the LFCC's thermal conductivity and mass loss rate under high temperatures. As shown in Figure 16(a), the thermal conductivity of LFCC decreases with the increase in temperature overall. However, in the middle stage, the thermal conductivity of some specimens first increases and then falls, such as YC-3, YC-4, YC-5, and YC-2. The main reason is that in the low-temperature stage of 25°C–150 °C, as temperature rises, the hydration products of cement increase, enhancing specimens' compactness and thermal conductivity. In the middle and high-temperature stage of 150°C–650 °C, the fibers dehydrate to shrink, and the cement matrix water evaporates. The cracks and pores increase in the specimens, reducing the thermal conductivity of the specimens. Some specimens, such as YC-1, YC-2, YC-5, and YC-6, increase their thermal conductivity when the temperature exceeds 500 °C. It is as a result of the cement matrix cracking, the severe cracking of leaf

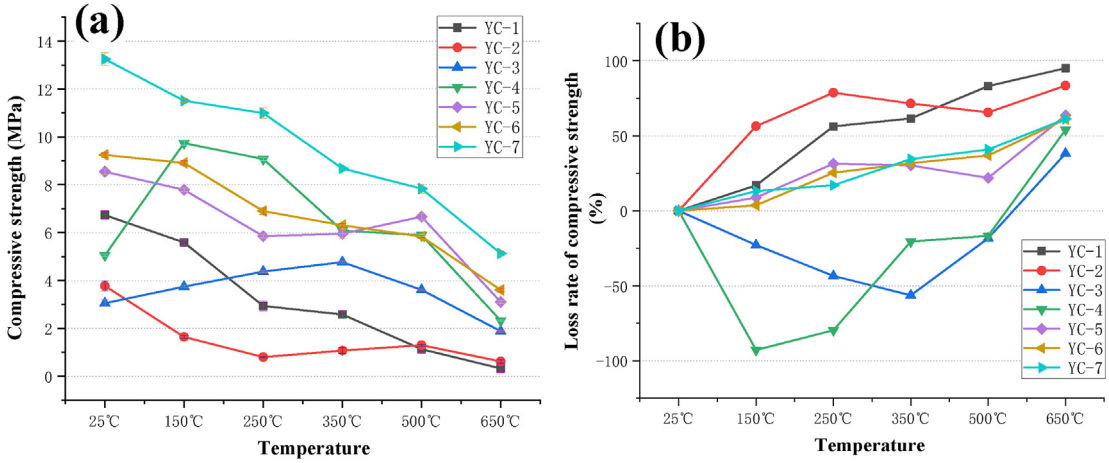


**Figure 14.** Compression strength and its loss rate of LFCC at high temperatures:(a) Compression strength; (b) Compression strength loss rate.

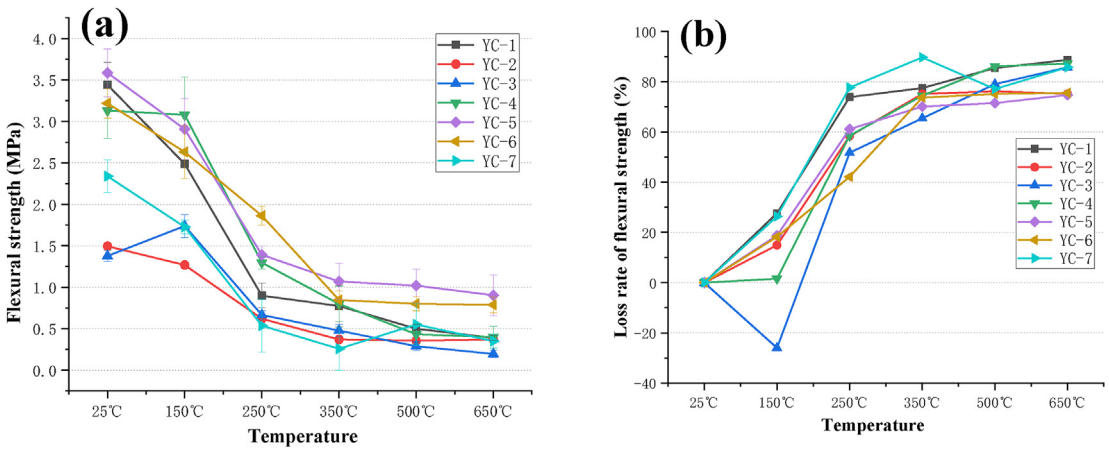


**Figure 15.** Flexural strength and its loss rate of LFCC at high temperatures:(a) Flexural strength; (b) Flexural strength loss rate.

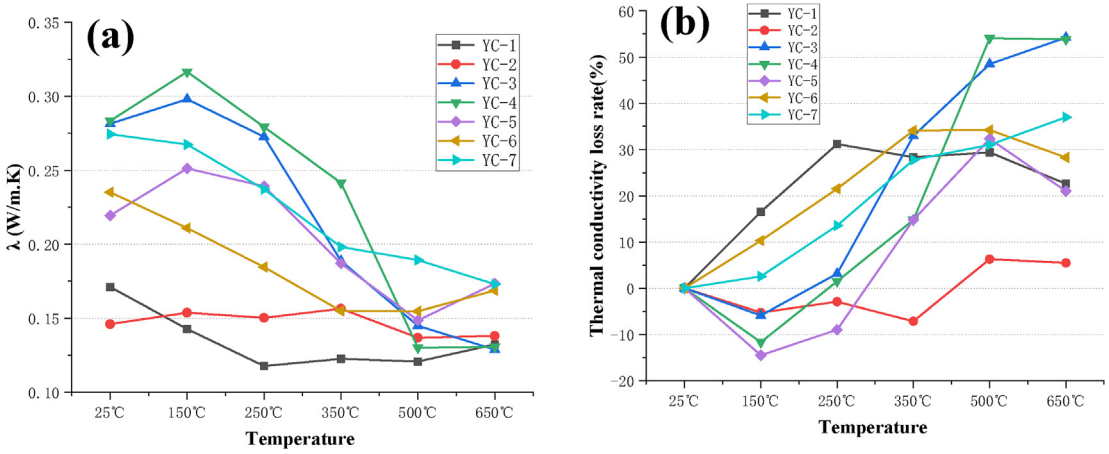


**Figure 16.** Thermal conductivity and its loss rate of LFCC at high temperatures:(a) Thermal conductivity; (b) Thermal conductivity loss rate.

fibers at high temps, and the increase of connecting pores, thus increasing specimens' thermal conductivity. At 650 °C, YC-3 and YC-4 have low thermal conductivity, which is 0.12881 (W/m.K) and 0.13073 (W/m.K), respectively, while YC-5, YC-7, and YC-6 have high thermal conductivity, which is 0.17330 (W/m.K), 0.17291 (W/m.K), and 0.16866 (W/m.K), respectively. It is because the thermal conductivity of LFCC is related to the thermal stability of fibers and the porosity and pore characteristics of the cement matrix [49]. When leaf fibers are modified with flame retardants, their surface porosity decreases, increasing the thermal conductivity of LFCC. Inevitably, during the LFCC molding process, some of the flame retardants MH and ATH are permeate into the cement-base materials, making the cement hydration products crisp and loose to a certain extent, and the porosity of cement matrix increases, thus reducing the thermal conductivity of composite material. Moreover, the latter played a more prominent role.

Figure 16(b) shows that, despite some specimens' loss rates of thermal conductivity decreasing at the middle and low temperatures stages, in general, the loss rate of thermal conductivity of the LFCC increases with the increase of temperature. This shows that the internal cracks and pores of LFCC specimen increase at high temperatures, and the thermal conductivity of the specimen decreases. At 650 °C, YC-3 and YC-4 have the largest loss rate of thermal conductivity, 54.22% and 53.87%, respectively, while YC-2 has the smallest loss rate, 5.47%. This further shows that MH and ATH with low solubility retain more on the fiber's surface when they modify the leaf fiber, which is easy to drain into the cement base material, increasing the number of interior pores of LFCC and affecting the hydration of the cement-based material at high temperatures. At the same time, APP with higher solubility is easier to penetrate the fiber when modifying leaf fiber, which has little impact on the hydration products of cement material. The internal pores of LFCC do not increase much under high temperatures.

### 3.5.4. *Micro-morphology of LFCC at high temperatures*

The micro-morphology of LFCC was examined using a scanning electron microscope (SEM) at 25 °C (a normal temperature) and 650 °C (a hot temperature), as illustrated in Figures 17 and 18, accordingly.

As shown in Figure 17, the leaf fibers in specimens have cement hydration products on their surfaces, which are mainly hydrated calcium silicate gel (C–S–H), in addition to two crystals of dicalcium silicate (2CaO•SiO2, C2S), tricalcium silicate (3CaO•SiO2, C3S), calcite (CaCO3), feldspar (Ca54MgAl2Si16O90), and the like [1, 2]. These hydration products are flocculent, massive, and granular forms and form a whole with fibers through adhesion and mechanical bite force. As a result of the fiber modification and LFCC molding process, fibers inevitably sustain damage and cracks, causing more pores to LFCC. There is a certain gap between fibers and cement-base materials caused by fibers' volume deformation during shrinkage. These pores will affect the strength and thermal insulation performance of LFCC. Generally speaking, the structure of YC-3 and YC-2 hydration products is loose. There are many pores and cracks in the hydration products, of which overall strength should not be high. The structure of hydration products in other groups is relatively dense, making the fibers and matrix well bonded. Since YC-7 is covered with sodium silicate, the amorphous silica gel becomes brittle and hard after hardening. Some cracks appear on the

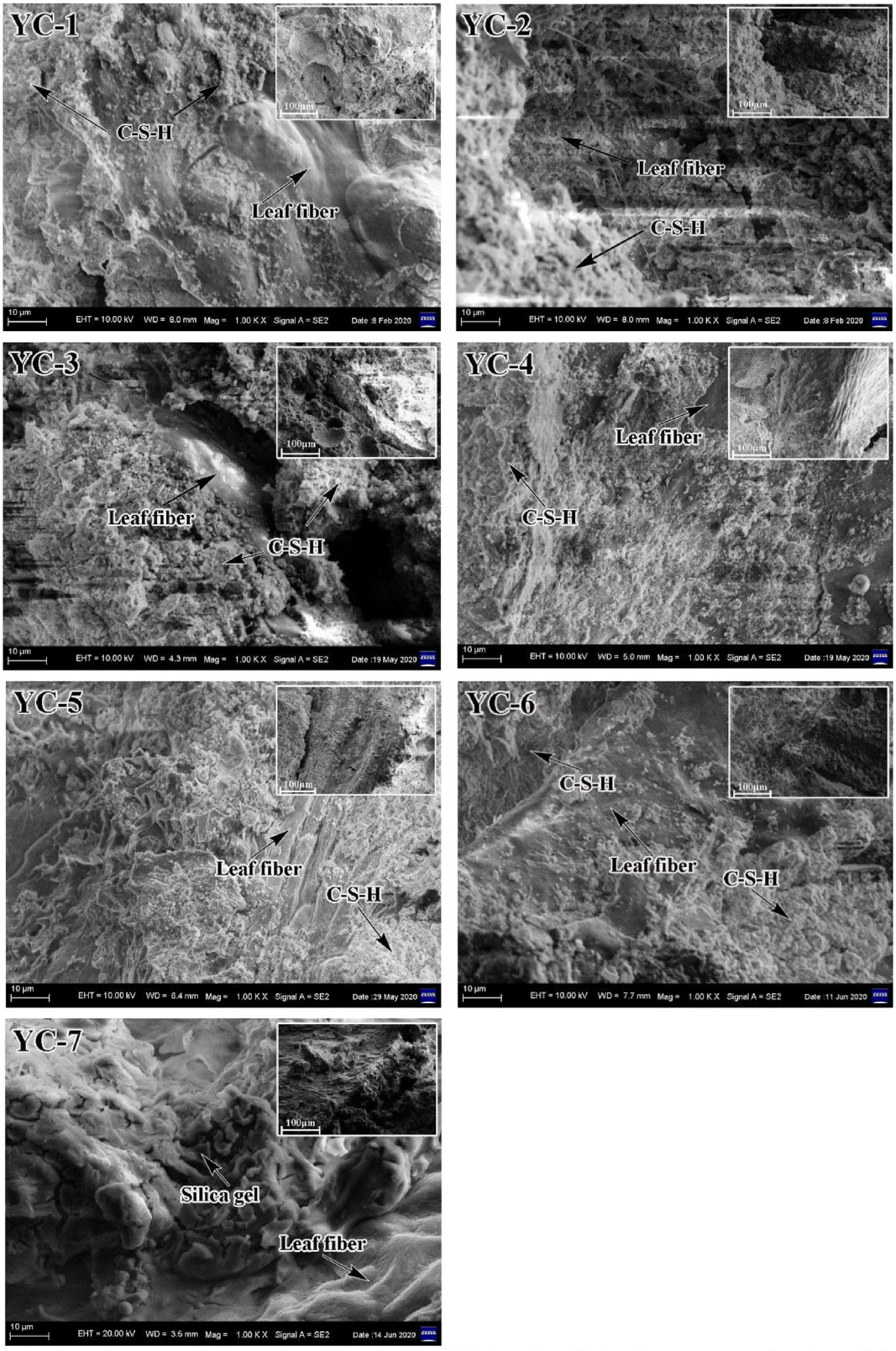


**Figure 17.** Micro-morphology of LFCC at 25 °C (1000 times): YC-1~YC-7 correspond to the serial numbers in Table 6.

surface of fibers, which will affect the bond strength between the fibers and the cement matrix to a certain extent. It can be seen from Figure 18 that after 650 °C, the leaf fibers in YC-1 and YC-2 are seriously carbonized. Other composite flame-retardant fiber samples are not entirely carbonized. Many cement hydration products have still adhered to the fiber surface. However, more needle-like particles are among the hydration products than at 25 °C, which is ettringite crystal (AFt) produced by cement hydration [50, 51]. Large fractures and pores on the outside and interior of the leaf fibers indicate that they have undergone thermal degradation and damage at high temperatures, fibers' ability to supply

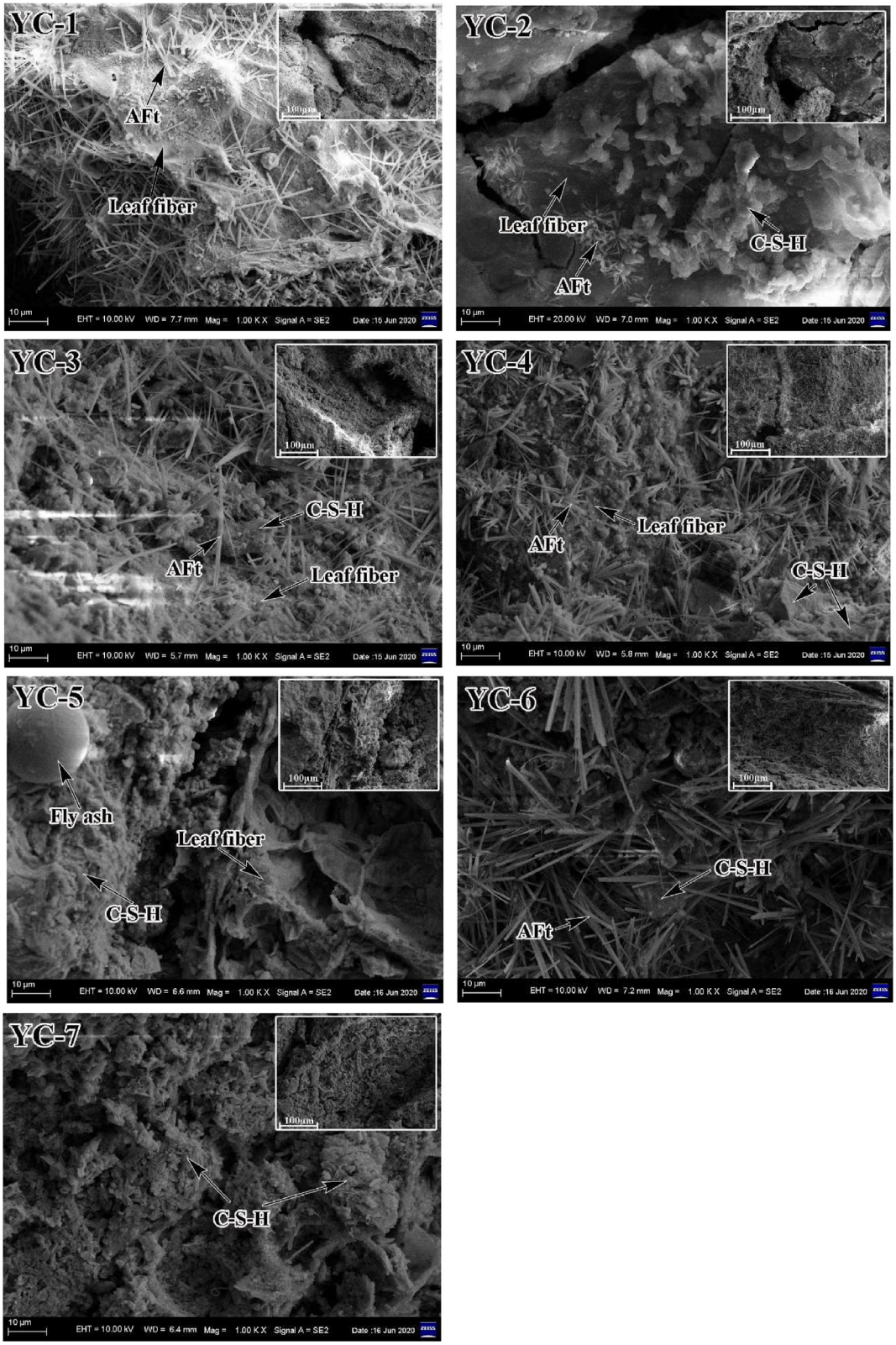


**Figure 18.** Micro-morphology of LFCC at 650 °C (1000 times): YC-1～YC-7 correspond to the serial numbers in Table 6.

the cement matrix with reinforcing and fracture resistance will inevitably decline. Cracks and defects that appear in the cement matrix under high-temperature stress will also reduce the strength of LFCC. YC-1, YC-2, and YC-3 hydration products have a crisp and loose structure. A poor bond between fibers and cement matrix results in low overall strength. The structure of hydration products in other groups is relatively dense, resulting in a tight bond between fibers and cement matrix.

#### 3.5.5. Discussion

Leaf fibers mainly comprise cellulose, hemicellulose, and lignin polymer compounds. When leaf fibers are heated, they undergo the first stage of moisture content separation. With the increase in temperature, hemicellulose and cellulose decompose to produce volatile products. Hemicellulose has a lower degree of polymerization than cellulose, an indefinite structure, and more inadequate thermal stability than cellulose, so it is relatively easy to be pyrolyzed. Lignin is an aromatic compound with insufficient chemical activity and relatively high decomposition temperature, most of which are decomposed into carbon [52].

The combustion of leaf fibers is a complex physicochemical process. The microscopic perspective is a free radical reaction process, including chain initiation, chain growth, and chain termination reaction. From the macroscopic point of view, the process results from the interaction of cellulose matrix, oxygen, and heat. Heat is the physical factor in realizing combustion, and oxygen is the chemical factor of combustion. The cellulose matrix is the material basis of combustion [53]. Therefore, the combustion process of leaf fibers is a free radical chain reaction process. The three factors work together, and this process is affected by many internal and external factors.

The combustion of leaf fibers can be divided into three stages [54]: ① thermal decomposition of cellulose matrix produces combustible gas; ② combustible gas burns in the air; ③ part of the heat generated by combustion causes the remaining cellulose matrix or molten material to continue to decompose, making the combustion continue. Therefore, to make the leaf fibers flame retardant is to terminate one or several stages of the combustion process. This process can usually be realized by the mechanism of condensed phase flame retardancy, gas-phase flame retardancy, and interruption of heat exchange [55, 56, 57].

Gas-phase flame retardant mechanism: when APP is decomposed by heating, it will produce ammonia, polyphosphate, and phosphorus oxides, as shown in the reaction Eqs. (1), (2), and (3). Ammonia will dilute oxygen, reduce the temperature of combustible gas, and inhibit the occurrence of flame combustion. When MH and ATH are decomposed by heating, it will produce a large amount of water vapor, as shown in reaction Eqs. (8) and (9), diluting the oxygen concentration on the leaf fibers' surface and slowing down or stopping the combustion reaction. Condensed phase flame retardant mechanism: phosphorus oxide and polyphosphoric acid in APP cover the surface of leaf fibers to inhibit the escape of combustible volatiles. As a strong dehydrating agent, polyphosphoric acid will dehydrate and carbonize leaf fibers to form a carbonization layer with oxygen isolation and heat insulation to play the role of flame retardant. After heating and dehydration, MH and ATH will form a metal oxide layer with a great specific surface area. The oxide layer will absorb smoke and combustible volatiles and cover the surface of leaf fibers to prevent oxygen and heat, stop the combustion chain reaction, and play the flame-retardant role. Interruption of heat exchange mechanism: in the decomposition of APP into phosphoric acid, the following reactions Eqs. (4), (5), (6), and (7) will happen to free radicals, which will capture O· radicals and prevent combustion. When the fiber is heated and burned, MH and ATH are heated to release crystal water, as shown in reaction Eqs. (8) and (9), which will absorb much heat to decompose and reduce the flame temperature.

$$(NH_4)_{n+2}P_nO_{3n+1} \rightarrow H_{3n}P_nO_{3n+1} + NH_3\uparrow \quad (1)$$

$$H_{3n}P_nO_{3n+1} \rightarrow (HPO_3)_n + nH_2O \quad (2)$$

$$(PO_3)_n \rightarrow P_2O_5 \text{ or } P_4O_{10} \quad (3)$$

$$H_3PO_4 \rightarrow HPO_2 + 5OH \quad (4)$$

$$PO\cdot + H\cdot \rightarrow HPO \quad (5)$$

$$HPO\cdot + H\cdot \rightarrow H_2 + PO \quad (6)$$

$$PO\cdot + OH\cdot \rightarrow HPO. + O. \quad (7)$$

$$2Al(OH)_3 \rightarrow Al_2O_3 + 3H_2O \quad (8)$$

$$Mg(OH)_2 \rightarrow MgO + H_2O \quad (9)$$

Although APP has a good flame-retardant effect, it will produce certain smoke (such as carbon monoxide) when the flame-retardant leaf fibers are burned. MH and ATH have the advantages of good flame-retardant effect, non-toxic and smoke reduction, with good thermal stability, helping them form, together with APP, a composite flame retardant. Multicomponent composite flame retardants have a co-action due to different flame-retardant mechanisms and decomposition temperature of each component, which is usually better than single component flame retardants (see 3.2.1 and 3.3).

## 4. Conclusions

We analyzed the thermal stability and flammability of leaf fibers in this paper, examined the mechanical and physical properties of LFCC at high temperatures, explored the fiber modification mechanisms with FTIR, TG/DTG, and SEM methods, and expounded the effects of modified leaf fibers on the properties of LFCC at high temperatures, and, on this basis, has drawn the following conclusions:

(1) The chemical functional groups of leaf fibers have been affected by the actions of three different types of flame-retardant modifiers and two different types of exterior coating layers, changing their chemical structure.

(2) Flame-retardant modified leaf fibers' thermal stability, with LOI larger than 27.0%, belongs to refractory materials, is much higher than that of the non-flame-retardant modified leaf fibers. The flame-retardant fibers Y7, Y3, and Y4 have good thermal stability with flame retardancy.

(3) The flame retardants components P, Mg, and Al are well deposited on the exterior of flame-retardant fibers, according to SEM and EDS examination. Agglomerated and debris flame retardants particles are also visible on the exterior of modified leaf fibers.

(4) At high temperatures, composite flame-retardant fiber LFCC has a lower mass-loss rate than non-flame-retardant or single-component flame-retardant fiber LFCC, in addition to YC-7.

(5) In general, at high temps, with temperature rises, the strength of LFCC decreases, the rate of strength loss is increases with the rise of temperature. At high temperatures, composite flame-retardant leaf fibers LFCC have an increased compression strength than fibers without flame-retardant modification or fibers modified with only one kind of flame-retardant, and their compression strength is lost at a slower pace. YC-5 and YC-6 have better strength at high temperatures among the composite flame-retardant leaf fibers LFCC.

(6) In general, the thermal conductivity of LFCC decreases with the increase in temperature, and its loss rate increases with the temperature rise. At 650 °C, YC-3 and YC-4 have low thermal conductivity, 0.12881 (W/m.K) and 0.13073 (W/m.K), respectively.

(7) At 650 °C, the leaf fibers in LFCC sustain thermal damage and thermal degradation at high temperatures. Many cement hydration products still adhere to the fiber surfaces, and the hydration products have more AFt crystals at 25 °C.

## Declarations

### Author contribution statement

Demin Jiang: Conceived and designed the experiments; Contributed reagents, materials, analysis tools or data; Wrote the paper.

Haodong Xu, Shuchen Lv, Di Jiang: Performed the experiments.

Suping Cui: Analyzed and interpreted the data.

Shiguo Sun, Xiaoruan Song: Contributed reagents, materials, analysis tools or data.

Shiqin He, Jingzong Zhang: Conceived and designed the experiments.

### Funding statement

Dr Jiang De-min was supported by Beijing Natural Science Foundation of China [2172021]. Xiaoruan Song was supported by North China University of Technology Yuyou Team Training Project [110052972027/027]. Shiguo Sun was supported by National Natural Science Foundation of China [41772335], 13th Five-Year National Key R&D Program "Research on Facilities Hazard Monitoring and Landslide Early Warning Standards" [2018YFF0213304], National Key R&D Program [2016YFC0701810], Innovative Engineering-Integration and Demonstration: Key Technology R&D Projects for Improving the Resilience Capability of Urban Rail Transit Infrastructure Disasters [2018–1].

### Data availability statement

Data included in article/supplementary material/referenced in article.

### Declaration of interests statement

The authors declare no conflict of interest.

### Additional information

No additional information is available for this paper.

## References

[1] F. Shukor, A. Hassan, M.S. Islam, M. Mokhtar, M. Hasan, Effect of ammonium polyphosphate on flame retardancy, thermal stability and mechanical properties of alkali treated kenaf fiber filled PLA biocomposites, Mater. Des. 54 (2014) 425–429.

[2] K. Ramanaiah, A.V. Ratna Prasad, K. Hema Chandra Reddy, Mechanical, thermophysical and flame properties of sansevieria fiber-reinforced polyester composites, Mater. Des. 49 (2013) 986–991.

[3] N. Li, H. Yan, L. Xia, L. Mao, Z. Fang, Y. Song, H. Wang, Flame retarding and reinforcing modification of ramie/polybenzoxazine composites by surface treatment of ramie fabric, Compos. Sci. Technol. 121 (2015) 82–88.

[4] D. Jiang, S. Cui, X. Song, J. Zhang, Analysis of micro-morphology and heat-insulating property of leaf concrete, Construct. Build. Mater. 49 (2013) 663–671.

[5] D. Jiang, P. An, S. Cui, F. Xu, T. Tuo, J. Zhang, H. Jiang, Effect of leaf fibers modification methods on mechanical and heat-insulating properties of leaf fibers cement-based composite materials, J. Build. Eng. 19 (2018) 573–583.

[6] L. Zhang, Z. Jiang, W. Zhang, S. Peng, P. Chen, Flexural properties and microstructure mechanisms of renewable coir-fiber-reinforced magnesium phosphate cement-based composite considering curing ages, Polymer 12 (2020) 2556.

[7] M.M. Camargo, E.A. Taye, J.A. Roether, D.T. Redda, A.R. Boccaccini, A review on natural fiber-reinforced geopolymer and cement-based composites, Materials 13 (2020) 4603.

[8] S. Jr Holmer, A. Vahan, Transition zone studies of vegetable fibre-cement paste composites, Cem. Concr. Compos. 21 (1999) 49–57.

[9] N. Padkho, A new design recycle agricultural waste materials for profitable use rice straw and maize husk in wall, Procedia Eng. 32 (2012) 1113–1118.

[10] D. Jiang, S. Cui, F. Xu, T. Tuo, Impact of leaf fibre modification methods on compatibility between leaf fibres and cement-based materials, Construct. Build. Mater. 94 (2015) 502–512.

[11] M. Ferrandez-Villena, C.E. Ferrandez-Garcia, T. Garcia-Ortuño, A. Ferrandez-Garcia, M.T. Ferrandez-Garcia, Analysis of the thermal insulation and flame-resistance capacity of particleboards made from vine (Vitis vinifera L.), Prunings. Polym. 12 (2020) 1147.

[12] Y. Xu, W. Li, M. Zhu, X. Yue, M. Wang, Novel porous fiber-based composites with excellent sound-absorbing and flame-retardant properties, J. Wood Chem. Technol. 40 (2020) 285–293.

[13] Z. Zhang, Z. Ma, Q. Leng, Y. Wang, Eco-friendly flame retardant coating deposited on cotton fabrics from bio-based chitosan, phytic acid and divalent metal ions, Int. J. Biol. Macromol. 140 (2019) 303–310.

[14] D. Jiang, S. Lv, S. Cui, S. Sun, X. Song, S. He, J. Zhang, P. An, Effect of thermal insulation components on physical and mechanical properties of plant fibre composite thermal insulation mortar, J. Mater. Res. Technol. 9 (6) (2020) 12996–13013.

[15] GB/T17671-1999, Method of testing cement—Determination of strength (ISO method), Chinese National Standard, 1999.

[16] GB/T10294-2008, Determination of Steady State Thermal Resistance and Related Properties of Insulation Materials—Protective Plate Method, Chinese National Standard, 2008.

[17] P. Acuña, J. Zhang, G.-Z. Yin, X.-Q. Liu, D.-Y. Wang, Bio-based rigid polyurethane foam from castor oil with excellent flame retardancy and high insulation capacity via cooperation with carbon-based materials, J. Mater. Sci. 56 (2021) 2684–2701.

[18] GB/T2406.2-2009, Plastics, Determination of Burning Behaviour by Oxygen index. Part 2: Ambient-Temperature Test, Chinese National Standard, 2009.

[19] GB/T 5454-1997, Textiles—Burning Behaviour—Oxygen index Method, Chinese National Standard, 1997.

[20] G. Tang, H. Jiang, Y. Yang, D. Chen, et al., Preparation of melamine–formaldehyde resin–microencapsulated ammonium polyphosphate and its application in flame retardant rigid polyurethane foam composites, J. Polym. Res. 27 (2020) 375.

[21] E. Asimakopoulou, J. Zhang, M. Mckee, K. Wieczorek, et al., Effect of layered double hydroxide, expanded graphite and ammonium polyphosphate additives on thermal stability and flame performance of polyisocyanurate insulation foam, Thermochim. Acta 693 (2020), 178724.

[22] X. Cao, H. Zhao, X. Liu, H. Luo, R. Liu, Preparation of petal-like magnesium hydroxide particles by adding sulfate ions, J. Cryst. Growth 550 (2020), 125841.

[23] T. Liu, F. Wang, G. Li, P. Liu, C. Gao, Y. Ding, S. Zhang, X. Kong, M. Yang, Magnesium hydroxide nanoparticles grafted by DOPO and its flame retardancy in ethylene-vinyl acetate copolymers, J. Appl. Polym. Sci. 138 (2021), 49607.

[24] S. Lan, L. Li, D. Xu, D. Zhu, Z. Liu, F. Nie, Surface modification of magnesium hydroxide using vinyltriethoxysilane by dry process, Appl. Surf. Sci. 382 (2016) 56–62.

[25] S. Gypser, F. Hirsch, A.M. Schleicher, D. Freese, Impact of crystalline and amorphous iron- and aluminum hydroxides on mechanisms of phosphate adsorption and desorption, J. Environ. Sci. 70 (2018) 175–189.

[26] F.Z. Arrakhiz, M. El Achaby, K. Benmoussa, et al., Evaluation of mechanical and thermal properties of Pine cone fibers reinforced compatibilized polypropylene, Mater. Des. 40 (2012) 528–535.

[27] T. Lu, S. Liu, M. Jiang, et al., Effects of modifications of bamboo cellulose fibers on the improved mechanical properties of cellulose reinforced poly (lactic acid) composites, Composites Part B 62 (2014) 191–197.

[28] K.Z.M. Abdul Motaleb, R. Al Mizan, R. Milašius, Development and characterization of eco-sustainable banana fiber nonwoven material: surface treatment, water absorbency and mechanical properties, Cellulose 27 (2020) 7889–7900.

[29] S.P. Kundu, S. Chakraborty, A. Roy, et al., Chemically modified jute fibre reinforced non-pressure (NP) concrete pipes with improved mechanical properties, Construct. Build. Mater. 37 (2012) 841–850.

[30] M.M. Kabir, H. Wang, K.T. Lau, F. Cardona, T. Aravinthan, Mechanical properties of chemically-treated hemp fibre reinforced sandwich composites, Composites Part B 43 (2012) 159–169.

[31] Y. Seki, M. Sarikanat, K. Sever, C. Durmuskahya, Extraction and properties of Ferula communis (chakshir) fibers as novel reinforcement for composites materials, Composites Part B 44 (2013) 517–523.

[32] K.V. Chalapathi, M.N. Prabhakar, J. Song, Impact of surface treatments and hybrid flame retardants on flammability, and thermal performance of bamboo paper composites, J. Nat. Fibers 10 (2020) 1–11.

[33] Y. Liu, H. Li, Q. Chen, F. Luo, C. Cao, Effect of bamboo flour on flame retardancy and smoke suppression of polypropylene/ammonium polyphosphate composites, Front. Mater. 9 (2020), 574924.

[34] S.P. Jozić, D. Jozić, J. Jakić, B. Andričić, Preparation and characterization of PLA composites with modified magnesium hydroxide obtained from seawater, J. Therm. Anal. Calorim. 142 (5) (2020) 1877–1889.

[35] N.H. Thi, T.N. Nguyen, H.T. Oanh, et al., Synergistic effects of aluminum hydroxide, red phosphorus, and expandable graphite on the flame retardancy and thermal stability of polyethylene, J. Appl. Polym. Sci. 11 (2020), 50317.

[36] C.H.S. Souza Rosa, M.G. Mothé, M.F.V. Marques, C.G. Mothé, S.N. Monteiro, Steam-exploded fibers of almond tree leaves as reinforcement of novel recycled polypropylene composites, J. Mater. Res. Technol. 9 (5) (2020) 11791–11800.

[37] R.F.P. Junio, L.F.C. Nascimento, L.M. Neuba, et al., Copernicia prunifera leaf fibers: a promising new reinforcement for epoxy composites, Polymer 12 (9) (2020) 2090.

[38] W. Zhang, C. He, Z. Wei, K. Shi, Impact of hot water treated Lotus leaves on interfacial and physico-mechanical of gelatin/Lotus leaf composites, J. Polym. Environ. 28 (12) (2020) 3270–3278.

[39] T.M. Loganathan, M.T.H. Sultan, Q. Ahsan, M. Jawaid, J. Naveen, A.U.M. Shah, L.S. Hu, Characterization of alkali treated new cellulosic fibre from Cyrtostachys renda, J. Mater. Res. Technol. 9 (3) (2020) 3537–3546.

[40] A.A. Silva, K. Dahmouche, B.G. Soares, The effect of addition of acrylic acid and thioglycolic acid on the nanostructure and thermal stability of PMMA–montmorillonite nanocomposites, Appl. Clay Sci. 47 (2010) 414–420.

[41] L. Yan, Z. Xu, N. Deng, Effects of polyethylene glycol borate on the flame retardancy and smoke suppression properties of transparent flame-retardant coatings applied on wood substrates, Prog. Org. Coating 135 (2019) 123–334.
[42] L. Song, W. Liu, F. Xin, Y. Li, Materials studio" simulation study of the adsorption and polymerization mechanism of sodium silicate on active silica surface at different temperatures, Int. J. Metalcast. 11 (2020).
[43] Q. Zhang, W. Lu, L. Zhou, D. Zhang, H. Cai, X. Lin, Tensile and flammability characterizations of corn straw slagging/high-density polyethylene composites, J. Thermoplast. Compos. Mater. 33 (11) (2020) 1466–1477.
[44] H. Chai, X. Tang, M. Ni, F. Chen, Y. Zhang, D. Chen, Y. Qiu, Preparation and properties of flexible flame-retardant neutron shielding material based on methyl vinyl silicone rubber, J. Nucl. Mater. 464 (2015) 210–215.
[45] L. Gu, Q. Yu, L. Zhang, Preparation and characterization of the halogen-free, smoke suppression, organic–inorganic hybrid flame-retardant expandable polystyrene materials, J. Appl. Polym. Sci. 137 (45) (2020), 49391.
[46] J. Tang, P. Li, X. Chen, Y. Bai, Experimental study of strength, pore structure and phase evolution characteristics of iron tailings cemented paste backfill under high-temperature, Cem, Wapno Beton 25 (2) (2020) 78–94.
[47] R. Štefan, M. Foglar, J. Fládr, K. Horníková, J. Holan, Thermal, spalling, and mechanical behaviour of various types of cementitious composites exposed to flame: experimental and numerical analysis, Construct. Build. Mater. 262 (2020), 119676.
[48] S. Zhang, X. Bu, X. Gu, J. Sun, H. Li, W. Tang, Improving the mechanical properties and flame retardancy of ethylene-vinyl acetate copolymer by introducing bis[3-(triethoxysilyl) propyl] tetrasulfide modified magnesium hydroxide, Surf. Interface Anal. 49 (7) (2017) 607–614.
[49] J.C. Mendes, R.R. Barreto, A.C.B. Paula, et al., On the relationship between morphology and thermal conductivity of cement-based composites, Cem. Concr. Compos. 104 (2019), 103365.
[50] M. Garg, A. Pundir, Investigation of properties of fluorogypsum-slag composite binders – hydration, strength and microstructure, Cem. Concr. Compos. 45 (2014) 227–233.
[51] H. El-Didamony, M. Heikal, K.A. Khalil, Characteristics of cement pastes containing sulphoaluminate and belite prepared from nano-materials, Construct. Build. Mater. 38 (2013) 14–21.
[52] P. Manimaran, G.P. Pillai, V. Vignesh, M. Prithiviraj, Characterization of natural cellulosic fibers from Nendran Banana Peduncle plants, Int. J. Biol. Macromol. 162 (2020) 1807–1815.
[53] T. Lee, Z.A. Zubir, F.M. Jamil, A. Matsumoto, F.-Y. Yeoh, Combustion and pyrolysis of activated carbon fibre from oil palm empty fruit bunch fibre assisted through chemical activation with acid treatment, J. Anal. Appl. Pyrolysis 110 (2014) 408–418.
[54] Y. Zhang, L. Wang, Y. Wu, Y. Chen, et al., Pyrolysis characteristics, kinetics, and its product characteristics of grape stem, Bioresources (4) (2019) 7901–7919.
[55] F.-Q. Zhang, B. Wang, Y.-J. Xu, P. Li, Y. Liu, P. Zhu, Convenient blending of alginate fibers with polyamide fibers for flame-retardant non-woven fabrics, Cellulose 27 (2020) 8341–8349.
[56] A. Thomas, M. Arun, K. Moinuddin, P. Joseph, Mechanistic aspects of condensed- and gaseous-phase activities of some phosphorus-containing flame retardants, Polymer 12 (2020) 1801.
[57] T. Ning, J. Zhang, L. Fu, Research advances of flame retardant polymer materials in the Field of electrical packaging, China Plast. Ind. 47 (10) (2019) 1–6, 147.